

Evidence of a massive planet candidate orbiting the young active K5V star BD+20 1790 [★]

M. Hernán-Obispo¹, M.C. Gálvez-Ortiz², G. Anglada-Escudé^{3,4}, S.R. Kane⁵, J.R. Barnes², E. de Castro¹, and M. Cornide¹

¹ Dpto. de Astrofísica y Ciencias de la Atmósfera, Facultad de Física, Universidad Complutense de Madrid, Avda. Complutense s/n, E-28040, Madrid, Spain
e-mail: mho@astrax.fis.ucm.es

² Centre for Astrophysics Research, Science & Technology Research Institute, University of Hertfordshire, College Lane, Hatfield, Hertfordshire AL10 9AB, UK

³ Department of Terrestrial Magnetism, Carnegie Institution of Washington, 5241 Broad Branch Road, NW, Washington, DC 20015-1305, USA

⁴ Departament d'Astronomia i Meteorologia, Universitat de Barcelona, Martí i Franqués 1, Barcelona, 08028. Spain

⁵ NASA Exoplanet Science Institute, Caltech, MS 100-22, 770 South Wilson Avenue, Pasadena, CA 91125, USA

received – ; accepted –

ABSTRACT

Context. BD+20 1790 is a young active, metal-rich, late-type K5Ve star. We have undertaken a study of stellar activity and kinematics for this star over the past few years. Previous results show a high level of stellar activity, with the presence of prominence-like structures, spots on the surface and strong flare events, despite the moderate rotational velocity of the star. In addition, radial velocity variations with a semi-amplitude of up to 1 km s^{-1} were detected.

Aims. We investigated the nature of these radial velocity variations, in order to determine whether they are due to stellar activity or the reflex motion of the star induced by a companion.

Methods. We have analysed high-resolution echelle spectra, by measuring stellar activity indicators, and computing radial velocity (RV) and bisector velocity spans. Also two-band photometry was obtained to produce the light curve and determine the photometric period.

Results. Based upon the analysis of the bisector velocity span, as well as spectroscopic indices of chromospheric indicators, like e.g. Ca II H & K, $H\alpha$, and taking into account the photometric analysis, we report that the best explanation for the RV variation is the presence of a sub-stellar companion. The Keplerian fit of the RV data yields a solution for a close-in massive planet with an orbital period of 7.78 days. The presence of the close-in massive planet could also be an interpretation for the high level of stellar activity detected. Since the RV data are not part of a planet search program, we can consider our results as a serendipitous evidence of a planetary companion. To date, this is the youngest main sequence star for which a planetary candidate has been reported.

Key words. stars: activity — stars: late-type — stars: individual (BD+20 1790) — stars: planetary systems

1. Introduction

Since the detection of the first planet orbiting a main sequence star, 51 Peg (Mayor & Queloz 1995), the radial velocity (RV) method has become the most successful technique for detecting exoplanets as the vast majority have thus far been discovered in this way (Udry & Santos 2007). This method is especially efficient for giant planets in close-in orbits owing to the large radial velocities they induce in the host star. The use of the RV

technique to detect exoplanets around young and active stars requires, in addition, a careful characterization of stellar activity. An active region on the stellar surface can produce changes in the shape of the spectral lines, thus inducing a subsequent temporal variation of the RVs that may mimic a planetary reflex motion with a period equal to the rotational period of the star (Saar & Donahue 1997). Some cases of false planetary detections are provided by Queloz et al. (2001), Bouvier et al. (2007), Huerta et al. (2008) and Huélamo et al. (2008). Thus the challenge in using the RV technique to detect young planets lies in disentangling the increased levels of stellar activity of young stars from the RV signals of the planets.

There is an absence of planets detected around stars younger than 100 Myr (Setiawan et al. 2007, Setiawan et al. 2008). Most RV searches for planetary companions have focussed mainly on stars older than 1 Gyr. Young stars were omitted from RV surveys until recently. Nevertheless, great effort has been made by several groups that have targeted young objects in their RV searches of planetary companions. For example, surveys are being carried out which focus on both nearby associations of young stars and moving groups with ages ranging 10–500 Myr;

[★] Based on observations collected at the German-Spanish Astronomical Center, Calar Alto, jointly operated by the Max-Planck-Institut für Astronomie Heidelberg and the Instituto de Astrofísica de Andalucía (CSIC). Based on observations made with the Italian Telescopio Nazionale Galileo (TNG) operated on the island of La Palma by the Fundación Galileo Galilei of the INAF (Istituto Nazionale di Astrofisica) at the Spanish Observatorio del Roque de los Muchachos of the Instituto de Astrofísica de Canarias. Based on observations made with the Liverpool Telescope operated on the island of La Palma by Liverpool John Moores University in the Spanish Observatorio del Roque de los Muchachos of the Instituto de Astrofísica de Canarias with financial support from the UK Science and Technology Facilities Council.

examples of which include β Pic (12 Myr), UMa association (300 Myr), Pleiades (100 Myr), IC 2391 (35 Myr), Hyades (700 Myr), Taurus association (2 Myr), ChaI (2 Myr), TWA (10 Myr) (Paulson et al. 2004, Paulson & Yelda 2007, Esposito et al. 2006, Huerta et al. 2007, Setiawan et al. 2007, Setiawan et al. 2008, Prato et al. 2008). Positive identification of planetary signatures from these efforts are few, with only two candidates to date: HD 70573 (Setiawan et al. 2007) and the controversial TW Hya (Setiawan et al. 2008). Planets orbiting around young stars are particularly valuable as they enable us to investigate some of the critical questions about the formation of both stellar and planetary systems. How, and at what stage planets form, what is the planet formation mechanism, and how they evolve are important questions which the study of young planetary systems will help to answer. In this paper we report strong evidence of a planetary candidate orbiting the young and active K5V star BD+20 1790. Sect. 2, is an overview of the properties and our previous studies of this star. The observational strategy and data analysis are presented in Sect. 3. In Sect. 4 the nature of RV variations is investigated. An orbital solution for the data is presented in Sect. 5, and in Sect. 6 a discussion about planetary parameters, orbital solution, and how stellar activity and the planet are related is shown. Finally, we summarize and offer some concluding remarks in Sect. 7.

2. BD+20 1790: An overview

BD+20 1790 was classified by Jeffries (1995) as a K5Ve star, with a magnitude of $V = 9.9$. Mason et al. (1995) identified this star as the optical counterpart for the 2RE J072343.6+202500 EUV source, located in the ROSAT All-Sky Survey. López-Santiago et al. (2006) proposed its membership in the AB Dor kinematic moving group which has an estimated average age of 50 Myr. By comparing the equivalent width of Li λ 6708 Å with the spectral type, López-Santiago et al. (2006) derived an age estimate of 35–80 Myr. The main stellar parameters for BD+20 1790 are compiled in Table 1. We obtained a value for the stellar radius from the measured rotational velocity and photometric period. Our estimated radius agrees with the previous K5V spectral classification (from Carrol & Ostlie (2007) tables). Adopting this spectral type, we used the K5V temperature from the Carrol & Ostlie (2007) tables. In conjunction with the photometric parameters, this enabled us to derive the luminosity, mass and surface gravity. Errors in the parameters were estimated by following the method of propagation of errors, i.e., the uncertainties were calculated from the errors in the variables involved in the determination of each parameter. It has been assumed null correlation between the different variables, in principle independent of each other. In order to test if assuming a fixed value for T_{eff} has a non-negligible effect in the errors computation, we investigated whether an error in T_{eff} could translate into uncertainties of derived parameters. We have considered an input error in $T_{\text{eff}} \sim 10$ K and conducted an analysis in the propagation of T_{eff} error. Based on this analysis, we have noticed that not consider the error in the T_{eff} leads to an underestimation in the errors in mass and $\log g$, providing unreliable error bars for these parameters.

The X-ray luminosity was calculated using the count rates and HR1 hardness ratios from the ROSAT All-Sky Survey. By combining the conversion factor C_x , computed by the formula from Fleming (1995), and the distance estimated by Reid et al. (2004), the stellar X-ray luminosity was calculated as $L_X = 1.6 \pm 0.5 \cdot 10^{29} \text{ erg s}^{-1}$.

We compute a preliminary value of metallicity by using a grid of Kurucz et al. (1993) ATLAS9 atmospheres and the 2002 version

of MOOG¹ synthesis code (Snedden 1973). Atmospheric models were constructed with the data given in Table 1. We used 12 Fe I lines selected from González et al. (2001). We also calculated a value of metallicity by using 7 Fe I lines in the MOOG Abfind routine. We find an average value of $A[Fe] = 7.82 \pm 0.20$ which, when assuming a solar value of $A[Fe] = 7.52$, results in a $[Fe/H] = 0.30 \pm 0.20$. As mentioned, this is a preliminary value, although compared with the average metallicity of stars of solar neighbourhood, we still could consider the star as metal-rich within the error bars.

In a recent paper Carpenter et al. (2008) derived the temperature, gravity and metallicity for BD+20 1790, being their values of $T_{\text{eff}} = 4408$ K and $\log g = 4.50$, very close to the corresponding values presented in Table 1. We also pointed out that the difference between metallicity values may be explained by the fact that Carpenter et al. (2008) only assumed a fixed metallicity of $[Fe/H] = 0.0$, but not actually compute it.

The Li I abundances analysis was also done in standard local thermodynamic equilibrium (ETL) using MOOG and ATLAS9 in the same way as with the metallicities. Abundances were derived by fitting synthetic spectra to the data. To determine Li abundances we perform a spectral synthesis around the Li I 6707 Å resonance doublet, fitting all spectra between 6702 and 6712 Å, taking into account the relation between Li6 and Li7 isotopes. We determine an average value of lithium abundance of $\log N(\text{Li}) = 1.03 \pm 0.04$ (where $\log N(\text{Li}) = \log(\text{Li}/\text{H}) + 12$).

In order to study the stellar activity and the kinematics, we have carried out both spectroscopic and photometric monitoring over the past few years: high temporal and spectroscopic resolution and two band photometry. The simultaneous study of photospheric and chromospheric active regions is a powerful tool that allow us to trace, reconstruct and model the puzzle of the magnetic field topology, since these active regions are the fingerprints of magnetic fields (Collier Cameron 2001, Catalano et al. 2002, Frasca et al. 2005, Collier Cameron et al. 2002). Strong chromospheric activity was detected in several observing runs, described by Hernán-Obispo et al. (2005, 2007). In spite of the fact that the rotational velocity is not very high, $v \sin i \sim 10 \text{ km s}^{-1}$ (López-Santiago et al. 2006), all activity indicators are in emission above continuum, from Ca II H & K, to Ca II IRT lines (see Fig. 1).

Through the study of profile line asymmetries of H α and H β lines, prominence-like structures have been detected in the chromosphere of the star (Hernán-Obispo 2005, 2007). These can be observationally detected as transient absorption features superimposed on the line profile that are interpreted as the presence of cool material embedded in the surrounding hotter corona and co-rotating with star (Collier Cameron & Robinson 1989a,b, Collier Cameron & Woods 1992, Jeffries et al. 1993, Byrne et al. 1996, Eibe et al. 1998, Barnes et al. 2000, Donati et al. 2001). Several completed prominence-like transients have been detected with durations of orders of a few hours (see Hernán-Obispo 2005 for details). Modeling these chromospheric phenomenae is an important challenge in this case, due to the detection of these prominence-like structures in unstable positions, far from equatorial regions (Ferreira 2000, Jardine et al. 2001, Jardine & van Balingoijen 2006).

In addition, strong large optical flare events were observed. The gradual decay of the flares was observed for up to 5 hours. Fig. 1 compares the activity indicators for the quiescent state and flare state. The energy released is on the order of $\sim 10^{37}$ erg,

¹ The source code of MOOG 2002 can be downloaded at <http://verdi.as.utexas.edu/moog.html>

Table 1. Stellar Parameters of BD+20 1790

Parameter	Value
Spectral Type	K5 V
$B - V$	1.15
M^a	$0.63 \pm 0.09 M_{\odot}$
T_{eff}^b	4410 K
$\log g^a$	4.53 ± 0.17
$EW(\text{Li})^a$	$110 \pm 3 \text{ m\AA}$
Distance ^c	$25.4 \pm 4 \text{ pc}$
Age ^c	35 - 80 Myr
$v \sin i^d$	$10.03 \pm 0.47 \text{ km s}^{-1}$
P_{phot}^a	$2.801 \pm 0.001 \text{ days}$
i^a	50.41 degrees
R^a	$0.71 \pm 0.03 R_{\odot}$
$[Fe/H]^a$	0.30 ± 0.20
$\log N(\text{Li})^a$	1.03 ± 0.04
L^a	$1.6 \pm 0.5 \cdot 10^{29} \text{ erg s}^{-1}$
L^a	$0.17 \pm 0.04 L_{\odot} \text{ erg s}^{-1}$

^a This paper

^b From Carrol & Ostlie, 2007

^c From López Santiago et al. 2006

^d From López Santiago 2005

^e From Reid et al. 2004

while for largest solar flares the released energy is about $\sim 10^{29}$ – 10^{32} erg, thus ranging the flares of BD+20 1790 on the so-called *superflare* regime (Rubenstein & Schaefer 2000).

The photometric observations yielded a light curve with evidence of rotational modulation, the semi-amplitude of which is up to $\Delta V \sim 0.^m06$ and indicates the presence of spots on the surface. The period analysis of the entire set of observations reveals a photometric period of 2.801 (± 0.001) days, in agreement with the period given by the SuperWASP photometric survey (Norton et al. 2007).

A detailed and completed study of the chromospheric and photospheric activity characterization will be published in a forthcoming paper (Hernán-Obispo et al. 2009b, in prep.).

3. Observations and Data Analysis

In order to study and characterize active regions at photospheric and chromospheric levels, we carried out photometric and spectroscopic observations of the target.

3.1. Spectroscopic data

The observational strategy was designed to spectroscopically monitor chromospheric activity indicators with high temporal and spectral resolution. High resolution echelle spectra were obtained during four observing runs, from 2004 to 2007, detailed in Table 2. The exposure times ranged from 900 s to 1200 s, depending on weather conditions, in order to obtain a S/N typically greater than 140 for SARG runs and 80 for FOCES runs. The spectra in the time series observations were separated only by the CCD readout time, thus enabling us to obtain the highest temporal resolution possible. Our initial temporal cadence was designed to detect prominence-like transient features in the Balmer lines. Spectral types and RV standards were acquired with the same setup and configuration as the target. These standards were reduced and analysed in the same way as the tar-

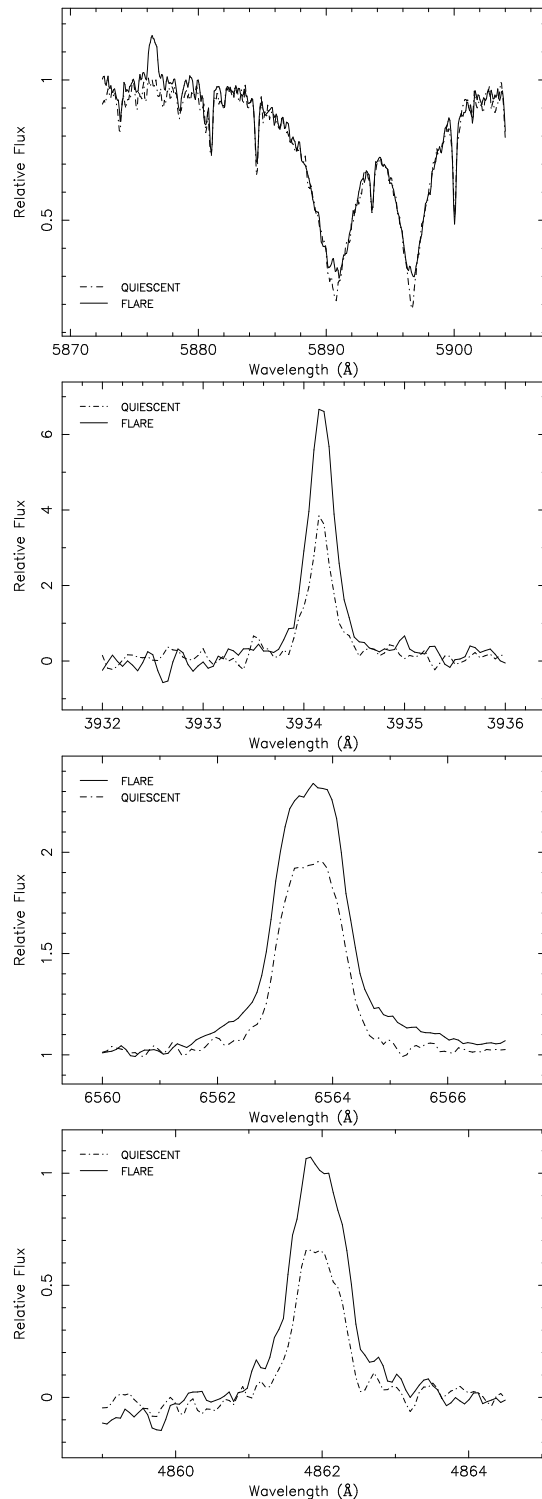


Fig. 1. Chromospheric activity indicators. The dashed line indicates quiescent state, while solid line indicates flare state. From top to bottom and left to right: He I D₃ region, Ca II K, H α and H β

get. The data were bias-subtracted, overscan-corrected and flat-fielded using standard routines in IRAF² package.

² IRAF is distributed by the National Optical Observatory, which is operated by the Association of Universities for Research in Astronomy, Inc., under contract with the National Science Foundation.

The wavelength calibration was obtained by taking spectra of a Th-Ar lamp. Using Coude spectrographs allowed a stable environment for the wavelength calibration, since flexures are not possible. Details about the spectrographs used can be seen in Pfeiffer et al. (1998) for FOCES spectrograph and Gratton et al. (2001) for SARG spectrograph. In order to enhance the accuracy in calibration we used about 10–12 lines identified per order; across all orders for SARG spectra and about 80 orders for FOCES spectra. The orders were calibrated simultaneously and the total fit has an rms value typically lower than 0.003 Å. The spectra were normalized by a polynomial fit to the observed continuum.

Heliocentric radial velocities were determined using a weighted cross-correlation method. The spectra of the star were correlated order by order against spectra of several RV standards with similar spectral type. Orders with chromospheric features and telluric lines were excluded. We calculated the uncertainties based on the cross-correlation peak height and the antisymmetric noise as described by Tonry & Davis (1979). Also, by measuring RVs of the standard stars, we estimated the systematic errors and the accuracy of the RV measurements with our instrumental setup. The accuracy between standards for the same run and between runs is less than 0.05 km s^{-1} .

Additional echelle data were acquired in DDT mode at the FOCES spectrograph on December 2008. The telescope configuration and the setup were identically to previous FOCES runs, except for two nights in which a different CCD was used. Data were taken over 10 consecutive nights but due to bad weather conditions only five nights were acquired. Because of the time limitation in DDT mode, only one RV standard was observed.

3.2. Photometric data

The purposes of these observations were to determine the photometric period and to look for photometric variability. In addition, the study of the light curve, as well as spectroscopy, allow us to characterize the active regions in the photosphere (Catalano et al. 2002, Frasca et al. 2005, Biazzo et al. 2007).

CCD differential aperture photometry was obtained using the 2.0 m fully robotic Liverpool Telescope (Steele et al. 2004) at the Observatorio del Roque de los muchachos in La Palma, Spain. The observations were scheduled in monitoring mode. We obtained 22 photometric epochs during November and December 2007. Our observational strategy permitted us to obtain a photometric epoch every 3 nights on average. Each epoch consisted in alternating r' and g' exposures³, thereby obtaining quasi-simultaneous two band photometry. Custom made software⁴ was used to automatically extract the photometry. By analysing intra night scatter we can infer a photometric accuracy of 3 mmag and 4 mmag per exposure (r' and g' bands respectively, see Fig. 2). We fit the best sine-wave model to the photometry sampling many periods between 0.1 and 50 days, on both bands. Plotting the post-fit residuals as a function of the period, a very strong minimum on the post-fit residuals is found at 2.801 ± 0.001 days in both bands (see Fig. 3). We note that the period and the amplitude are similar with those given by the SuperWASP survey (Norton et al. 2007).

The different amplitude in each band is consistent with large spot or spot group covering at least 4% of the surface. As can be seen in Fig. 2, the amplitude is larger at shorter wavelength, i.

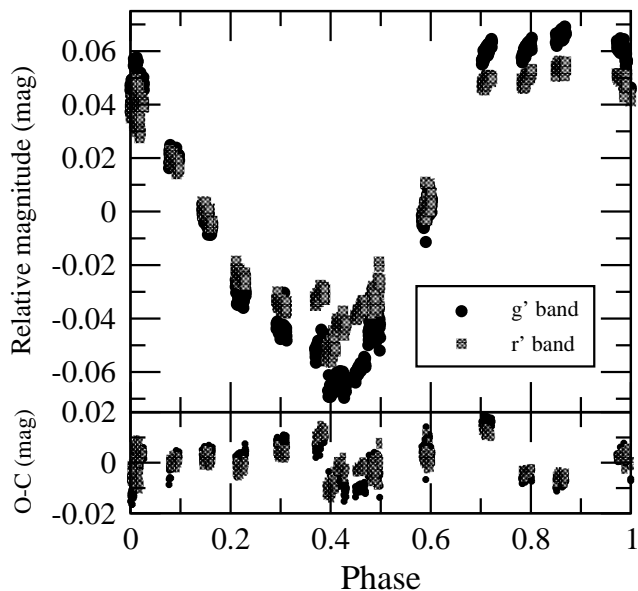


Fig. 2. Photometry phased to the 2.801 days period. A linear trend and a zero point have been subtracted to both bands. The residuals with respect to a simple sine-wave model are shown in the lower panel.

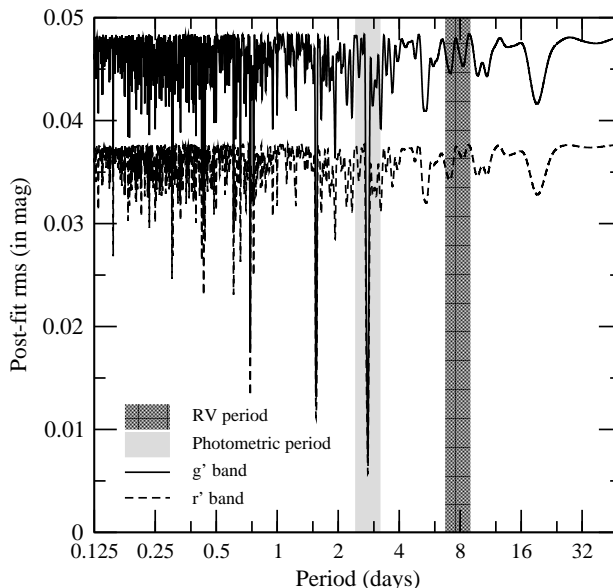


Fig. 3. Postfit residuals to the photometry as a function of the period. The sharper minima correspond to the 2.801 days period in both bands. The RVs period is marked in grey to illustrate the absence of related photometric signals.

e. at g' band in this case. This color variation is correlated with variation in magnitude. The star appears redder when fainter, at minimum light and therefore bluer when brighter, at maximum light.

The full analysis of the photometry and its relation to the star activity requires simultaneous discussion with the spectroscopic data and a more detailed study of the star will be presented elsewhere (Hernán-Obispo et al. 2009b, in prep.)

³ Sloan r' and g' filters were used

⁴ ATP, Automatic TATOOINE Photometry.
http://www.am.ub.es/~anglada/atp/atp_testing.htm

Table 2. Observing runs

Date	Telescope	Instrument	CCD chip #	Spect. range (Å)	Orders	Dispersion (Å/pix)	FWHM ^c (Å)	N. Obs.
29/03-6/04 2004	2.2m ^a	FOCES	2048x2048 24μm Site#1d	3720 - 10850	100	0.04 - 0.13	0.08 - 0.35	19
21-22/11/2004	TNG ^b	SARG	2048x4096 13.5μm EEV	4620 - 7920	52	0.07 - 0.11	0.07 - 0.17	43
15/04/2006	TNG ^b	SARG	2048x4096 13.5μm EEV	4620 - 7920	52	0.07 - 0.11	0.07 - 0.17	14
2-5/10/2007	2.2m ^a	FOCES	2048x2048 24μm Site#1d	3720 - 10850	100	0.04 - 0.13	0.08 - 0.35	10
12-13/12/2008	2.2m ^a	FOCES	2048x2048 15μm LORAL#11i	3830 - 10850	96	0.03 - 0.07	0.09 - 0.26	2
19-21/12/2008	2.2m ^a	FOCES	2048x2048 24μm Site#1d	3620 - 7360	100	0.04 - 0.13	0.08 - 0.35	3

^a 2.2 m telescope at the German Spanish Astronomical Observatory (CAHA) (Almería, Spain).

^b 3.58 m *Telescopio Nazionale Galileo* (TNG) at Observatorio del Roque de los Muchachos (La Palma, Spain).

^c The spectral resolution is determined as the FWHM at the arc comparison lines ranges.

4. On the nature of the RV variations

Variations in the RV peak-to-peak amplitude of up to $\sim 2 \text{ km s}^{-1}$ were observed during all the observing runs. These variations are significantly larger than the individual measurement errors (0.10 to 0.20 km s^{-1}) or the systematic error (0.05 km s^{-1}), even when we consider the scatter between runs with different spectrographs and setups.

4.1. Searching for periodical signals on RV

A Least squares periodogram (see Appendix A) reveals one very significant peak at 7.783 days (see Fig. 4a). The data set contains 91 independent RV measurements. However, many of them are clustered together within groups of a few hours. The values we use to generate the periodogram and for orbital fitting (shown in Table 3), are averaged on a nightly basis. Fig. 4b shows the empirical False Alarm Probability (FAP) as a function of the Power. The 7.783 days peak has a FAP of 0.35%.

It is worth noting that the RV period is larger than the photometric period. Nevertheless to test if the RV period could arise from rotational modulation we searched for significant frequencies in the data points of the photometry. There is no significant power at the RV period, and no secondary peaks are found in the aliasing frequencies of the RVs or the photometric period after the main signals are removed. To illustrate the absence of related photometric signals, we marked the RV period in Fig. 3, that shows the post-fit residuals of photometric data. In addition to this, there is no signal at photometric period in the RV data, as can be seen in Fig. 4a, that shows the RV periodogram.

4.2. Stellar activity jitter

It is well known that spurious RV variations can be induced by stellar activity, especially due to changes in the profile of spectral lines caused by the presence of active regions, the so-called *stellar jitter* (Saar & Donahue 1997, Saar 2009). The high level of activity detected in BD+20 1790, induced us at first to relate RV variations with active regions. Since we ruled out the possibility of variations due to systematic errors or any seasonal effect, the main concern was to determine if stellar activity was responsible.

It is widely accepted that the relationship of bisectors of the cross-correlation function (CCF) and RV is a powerful method to determine whether the RV variation may be due to stellar activity or a planetary companion (Queloz et al. 2001, Martínez-

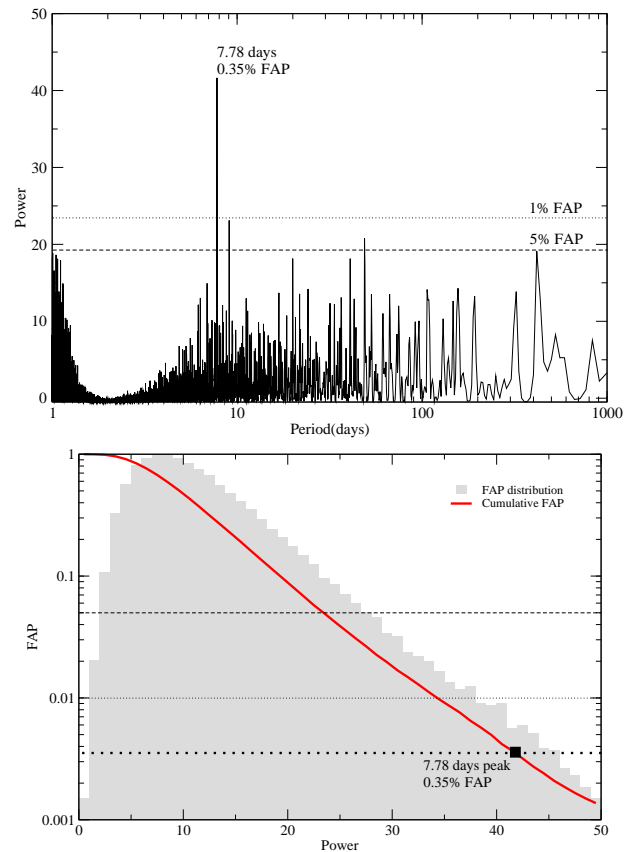


Fig. 4. a. Up: Least-Squares Periodogram of the nightly averaged radial velocity measurements. The 7.78 days peak has a FAP of 0.35%. The dotted horizontal line illustrates a FAP lower than 1% and the dashed horizontal line a FAP lower than 5%. **b. Down:** Empirical False Alarm Probability as a function of the Power (red line). The gray bars illustrate the distribution of False Alarms with an arbitrary normalization used to derive the Empirical FAP. Note that the Y axis is in logarithmic scale.

Fiorenzano et al. 2005). The CCF was determined by using the same procedure as for the RV case, computing it for the regions which include the photospheric lines which are more sensitive to spot presence, while excluding chromospheric lines and telluric lines. The bisector inverse slope (BIS), defined as the difference of the average values of the top and the bottom zones, was computed to quantify the changes in the CCF bisector shape by us-

Table 3. Radial Velocity

JD days	RV (km/s)	σ (km/s)
2452388.3341 ^a	9.23	0.19
2452389.3513 ^a	8.94	0.14
2452390.3670 ^a	8.52	0.38
2453099.3573 ^a	7.82	0.06
2453100.3692	6.96	0.10
2453101.3748	7.34	0.07
2453102.3876	7.84	0.05
2454375.6480	7.96	0.08
2454378.6804	7.72	0.04
2453331.6400	8.71	0.03
2453332.6800	8.16	0.03
2453841.4250	7.73	0.03
2454812.7429	7.76	0.21
2454813.7240	7.67	0.18
2454820.5057	7.73	0.16
2454821.5126	7.53	0.16
2454822.5483	7.96	0.14

^a From López-Santiago 2005

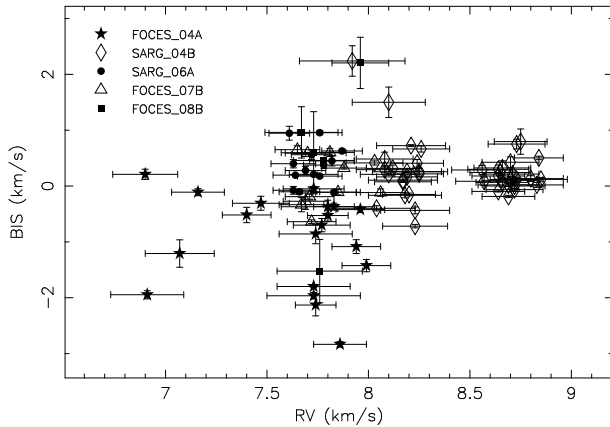


Fig. 5. Bisector velocity span vs. Radial velocity for all the observing runs. Symbols represent the different runs: stars for FOCES 04A, diamonds for SARG 04B, circles for SARG 06A and triangles for FOCES 07B. The lack of correlation indicates that RV variations are not due to stellar activity.

ing the method described by Queloz et al. (2001). In choosing the span zones we avoided wings and cores of the CCF profiles, where errors of bisectors measurements are large. In Fig. 5 it can be seen that there is a lack of correlation between the BIS and RV variation for all the observing runs. This indicates that the RV variations are not due to variations in the asymmetry of the photospheric lines profile, and subsequently not due to stellar activity variations. The least squares periodogram of bisectors shows two tentative peaks around 2.8 days, and is shown in Fig. 6.

We have estimated the stellar jitter from Santos et al. (2000), that takes into account the Ca II H & K index. Assuming an average value for Ca II H & K index of about -4.2 and by using eq. [4], we derived a value for the stellar jitter of up to 10 m s^{-1} . This stellar jitter is added in quadrature to the RV error.

As an additional test we investigated the variation of stellar activity indicators, especially those that are ascribed to the presence of plage-like structures on the chromosphere, like Balmer lines, Ca II H & K and Ca II IRT. The emission flux for these lines in active stars usually shows a periodic modulation (and

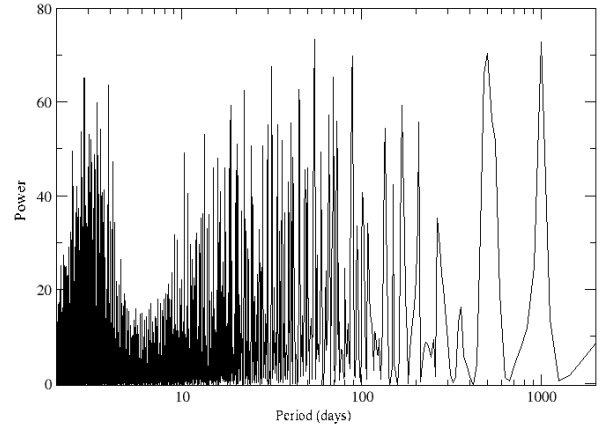


Fig. 6. Periodogram for bisectors of all runs. There is no clear period for bisector variations.

subsequently the spectroscopic indices) which is most likely due to rotational modulation of plage-like structure emission. As is shown in Sect. 2, all chromospheric activity indicators are in emission above the continuum, indicating a very high level of activity. To avoid the photospheric contribution to the spectral profiles we applied the spectral subtraction technique described in detail by Montes et al. (1995). This technique makes use of the program STARMOD developed at Penn State University (Barden 1985) and lately modified by Montes et al. (1995). Also, in order to control the error and minimize the uncertainties, some routines of the astronomical data reduction package REDUCE⁵ developed at Universidad Complutense de Madrid (Cardiel 1999) were used. In these subtracted spectra, spectroscopic indices have been defined and computed following Saar & Fisher (2000), Küster et al. (2003), Bonfils et al. (2007). Both, Ca II IRT and Ca II H & K indices were only determined for FOCES runs, due to the wavelength range coverage of the spectrograph. To avoid contamination from telluric lines we only consider the 8662Å Ca II IRT line. We searched for periodic signals in the spectroscopic indices by computing their Least squares periodograms. Fig. 7 shows the variation with time (orbital phase folded in this case) for Ca II IRT, Ca II H & K, H α and H β indices. The corresponding periodogram computed shows more noise rather than a clear signal. This result is also seen in the indices figures as a non-modulation of the activity index. As an example, Fig. 8 shows the periodogram for the H α index.

As pointed out by Walter (1994), the rotational modulation of chromospheric lines due to plages is not always detectable in very active stars. Furthermore, in this case the flares could contaminate the data, masking the actual period of variation of the indices. In order to investigate this possibility we removed the data affected by flare events. Due to the different wavelength range coverage of spectrographs, we considered only H α and H β indices. For H α index, we have found a tentative rotational modulation with a period of 2.77 days, similar to photometric period (see Fig. 9). However, the postfit residuals show in Fig. 10 that this could be a misleading signal, even pure noise. For H β index, no clear modulation has been found.

The lack of variability of BIS and spectroscopic indices with RV

⁵ <http://www.ucm.es/info/Astrof/software/reduceme/reduceme.html>

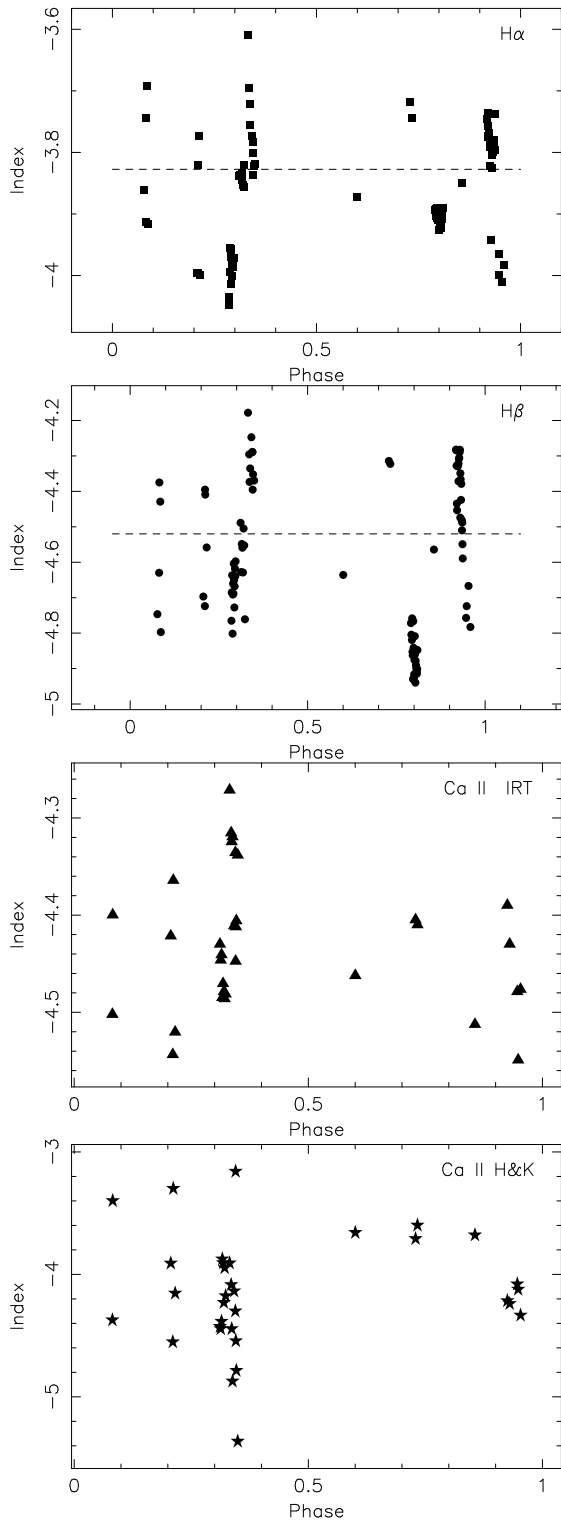


Fig. 7. Spectroscopic index for chromospheric activity indicators, phased folded orbital period. From top to bottom: $H\alpha$ (squares), $H\beta$ (circles), Ca II IRT (triangles) and Ca II H \& K (stars). The dashed line is indicating the quiescent state. Error bars for indices are of order of 0.001

period, and the absence of a photometric period larger than 2.8 days, strongly support the planetary companion hypothesis.

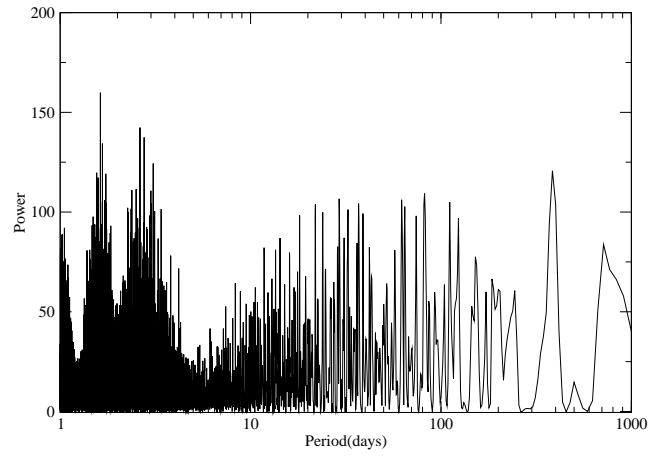


Fig. 8. Periodogram for $H\alpha$ index. There is no clear period for index variations.

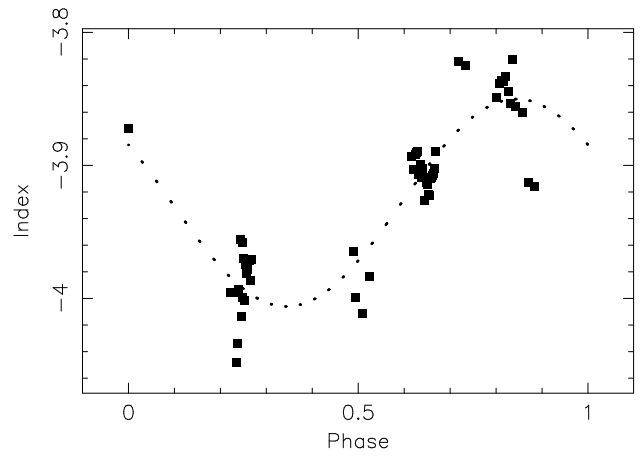


Fig. 9. $H\alpha$ index for the data without flare events. It can be seen a modulation with a period of about 2.77 days, similar to photometric period.

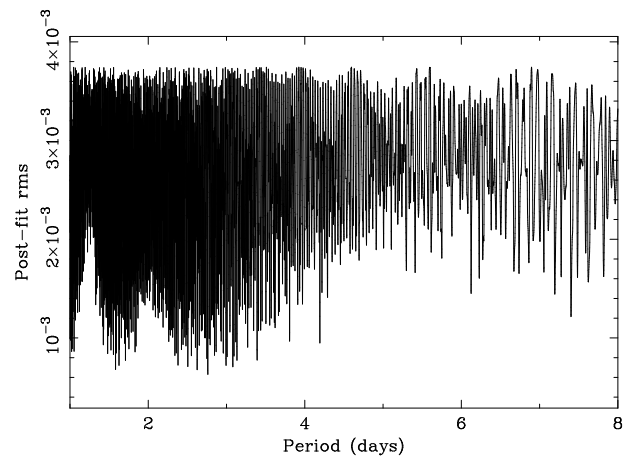


Fig. 10. Postfit residuals to $H\alpha$ index for no-flare data as a function of the period. There is no clear period for index variations.

4.3. RV wavelength dependence

Desort et al. (2007) (hereafter D07) pointed out that the color dependence (with wavelength) of the RV peak-to-peak amplitude with spots can be used as a diagnostic to discriminate between stellar activity or planetary companions. Due to the contrast be-

tween spots and the surrounding photosphere being greater in the visible than at IR wavelengths, it is expected that an attenuation of RV amplitude towards red wavelengths would be seen. Observationally this effect has been shown by e.g. Martín et al. (2006), Huélamo et al. (2008) and Prato et al. (2008). If the RV variations are due to a planet, the RV amplitude should be the same at every wavelength range. We investigated a possible chromatic dependence by computing the RV in two different ranges of wavelength, one for red and near-IR wavelengths (7650 to 10000 Å) and the other for blue (4300 to 4800 Å). The resulting RV peak-to-peak amplitude is $2.19 \pm 0.20 \text{ km s}^{-1}$ for the near-IR range and $2.20 \pm 0.20 \text{ km s}^{-1}$ for the blue range. The values differ by only 0.5% and agree within the uncertainties. Additional RV infrared follow-up can allow us to confirm this. In a forthcoming paper (Hernán-Obispo et al. 2009d, in prep.), we will present the first results of the study of the RVs of BD+20 1790 in the near-IR range.

4.4. RV variation by empirical spots and plages?

To estimate an order of magnitude of the expected RV amplitude due to spots, we use empirical relations derived by Saar & Donahue 1997 (hereafter SD97) and D07. These relations connect the RV amplitude with the spot filling factor f_s and $v \sin i$. We consider both relations by D07 and SD97, because D07 relations take into account the spectral type and the whole spectral range (except telluric and chromospheric lines) to compute the empirical RV, whereas SD97 uses a single line and G5V spectral type. Using SD97 eq. [1], we derived an amplitude of up to 575 m s^{-1} and by using D07 eq [5] we similarly estimate an amplitude of up to 600 m s^{-1} . As mentioned, these results are taken as a quantitative estimation. There are more effects that are not taken into account here, like the spot location at stellar surface given by the colatitude θ , and the spot temperature. SD97 eq. [1] and D07 eq. [5] considered the simple case of an equatorial spot, but SD97 assumed a $T_{spot} = 0 \text{ K}$ and D07 assumed an spot temperature 1000 K cooler than the photosphere. The difference between the RV amplitude derived from both equations could be due to this different spot temperature.

On the other hand, we can estimate the spot filling factor that could produce the RV signal of our data. We considered an average semi-amplitude of 1 km s^{-1} . The f_s estimated from SD97 is therefore 23% while D07 indicates 19%. The f_s measured from photometric variation is about 4%. These results indicate that the spot filling factor needed to explain the RV variation due purely to spots is not in agreement with the photometry.

Saar (2003) and Saar (2009) showed significant efforts to model plage-induced RV jitter. Although the models are mostly applicable to solar-like stars, we could estimate the plage filling factor f_p that could produce the RV signal by using the Saar (2009) equation that connects the RV amplitude with $v \sin i > 6 \text{ km s}^{-1}$. This f_p estimated is about 70%, that strongly suggests that the RV variation is not due to chromospheric plages.

4.5. What would the RV signal be without a planet?

It is important to remark that empirical relations derived by SD07 and D07 do not take into account the chromatic effect of spots on the RV signal. We therefore investigated how much RV signal would be expected in the absence of a planet, and the degree of RV attenuation with wavelength (assuming the RVs are due to cool spots). In order to quantify the attenuation if the cause of variations were spots, we try to investigate how much

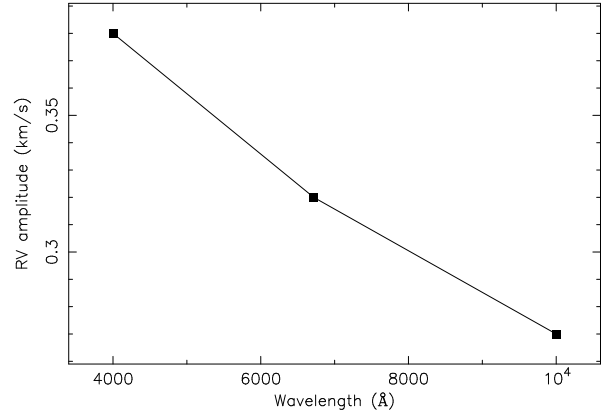


Fig. 11. Radial velocity amplitude variation with wavelength, computed for LO Peg profiles

spots affect the line profiles. However, BD+20 1790 has a low $v \sin i$ to model the photosphere by generating Doppler imaging spot maps. To carry out a realistic approximation to the problem, we construct realistic spot maps by using spectra of another star with similar characteristics, LO Peg, that is widely studied in the literature and its photospheric activity is well-known (Jeffries & Jewell 1993, Jeffries et al. 1994, Eibe et al. 1998, Eibe et al. 1999, Barnes et al. 2005). LO Peg is a K5V–K7Ve star, identified by Jeffries & Jewell (1993) as a member of the Local Association, with an estimated age of 20–30 Myr. Jeffries et al. (1994) determined the inclination to be 50° . The level of activity is similar to BD+20 1790, but LO Peg is a rapid rotator ($v \sin i \sim 69 \text{ km s}^{-1}$). The LO Peg photometry suggests a spot filling factor of up to 1.5%.

Using the Doppler imaging program, DoTS (Collier Cameron 1997), and an input starspot image derived for LO Peg (Barnes et al. 2005), we generated a set of line profiles for a star with $v \sin i = 10 \text{ km/s}$ (i.e. matching that of BD+20 1790) over a complete rotation phase. The profiles thus contain asymmetries due to starspots from the observed LO Peg image. We used appropriate temperatures for the BD+20 1790 photosphere and estimated the spots to possess temperatures which were up to 1000 K cooler. Profiles were generated for the three different wavelengths of 4000 Å, 6717 Å and 10000 Å. The radial velocity variations were then calculated in order to estimate the relative amplitudes due to spot induced variations at each of the three wavelengths.

The RV attenuation with wavelengths relative to 4000 Å is 16% at 6717 Å and about 30% at 10000 Å, as illustrated in Fig. 11. Assuming at a first approach the same f_s for LO Peg and BD+20 1790, the RV signal for BD+20 1790 should be about 1.5 km s^{-1} at 10000 Å.

However, in Hernán-Obispo et al. 2009d (in prep.), we find only about 0.5% attenuation in the near-IR region relative to the visible, 6717 Å region. This result is an additional argument in support the existence of the planetary companion.

4.6. RV jitter from flares

We have estimated the rate of flare occurrence as the fractional amount of the total observing time (for all runs) where a flare was detected. Thus, we get a flare frequency of occurrence of $\sim 40\%$. This higher rate raises the question of how much RV jitter we should expect from large flares, if any. Saar (2009) presents the first approach to this issue, concluding that RV jitter due to

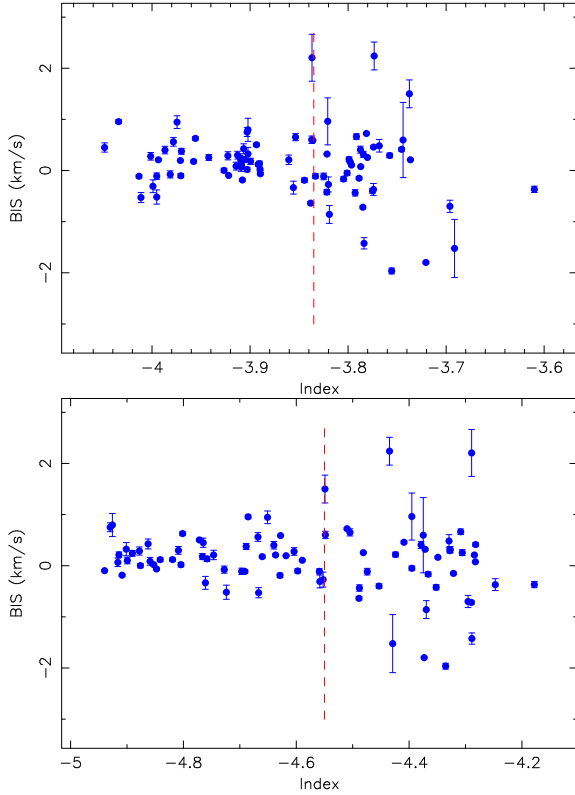


Fig. 12. Up: $H\alpha$ index vs. BIS. The dashed line is indicating the quiescent state. **Down:** $H\beta$ index vs. BIS. For both, it is seen that the scatter for BIS is higher when occur flare events. Error bars for the indices are of order of 0.001.

flare occurrence would be non-negligible, although probably be a stochastic jitter component. Chromospheric activity indicators exhibited an enhancement at flare state, the broad emission of Balmer lines and He I D_3 in emission being the most notable features (see Fig. 1). As pointed out by Saar (2009), although these lines are excluded when we measure RV, it is possible that a significant core filling in photospheric lines occurs when there is a flare event. The cause could be upper photospheric heating. Results by Houdebine (1992) state that heating is propagated down to low photospheric levels.

A second related problem is the effect of large flares on BIS. While it has not been studied until now, it is expected to be more pronounced, since bisectors are more sensitive to changes in line profiles. To our knowledge it is reported here for the first time. Fig. 12 a shows the relationship of $H\alpha$ index vs. BIS, where the dashed line corresponds to the quiescent state, and higher values for $H\alpha$ index indicate the occurrence of a flare event. It is seen that the scatter for BIS is higher when a flare occurs. Outliers at quiescent state correspond to a low S/N rate. Similar BIS behaviour is seen in Fig. 12 b, that shows $H\beta$ index vs. BIS.

5. Orbital solution for BD+20 1790 b

We computed the orbital solution for the RV data using a standard Keplerian fit with the RV period estimated by the Least squares periodogram. The fit was obtained firstly only considering the FOCES data, averaged by night, in order to avoid intra-night scatter. After this, we added the SARG data to improve the fit. The results for the fit considering only FOCES data or all data from the two spectrographs were compatible within uncertainties. With the addition of RVs measured in winter 2008

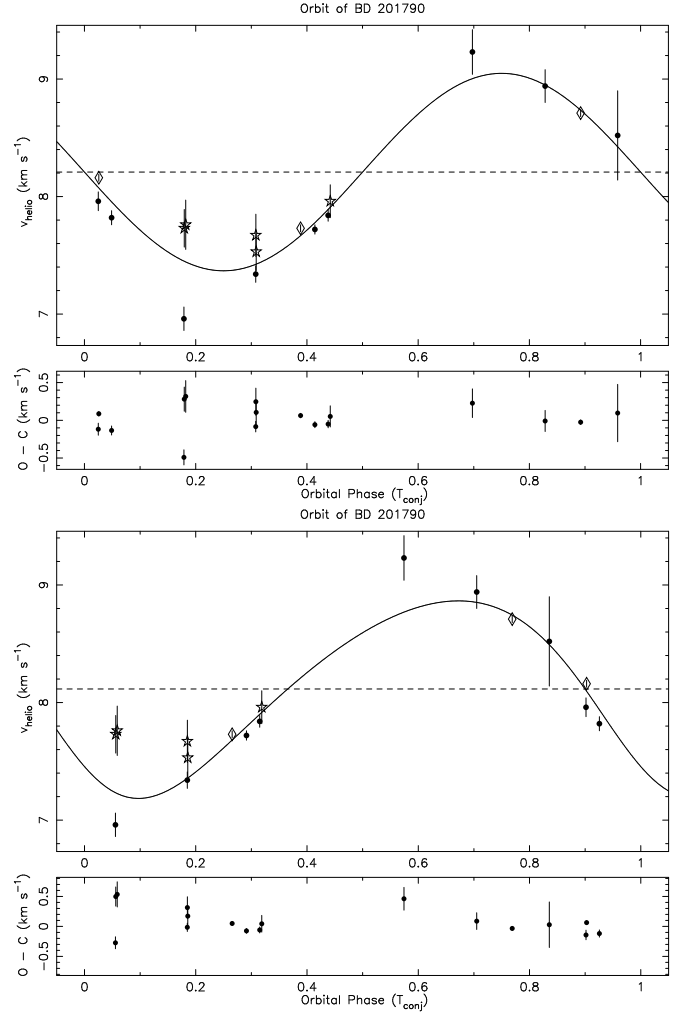


Fig. 13. Radial velocity variability of BD+20 1790.a. Up: Circular orbit. **b. Down:** Eccentric orbit. Values marked with circle symbol represent FOCES runs except stars that represent DDT FOCES 08B run. Diamond symbol are for SARG runs.

(DDT FOCES 08b run), the Least squares periodogram is strikingly improved, and the 7.78 day peak clearly dominates the power spectrum. Attempts to perform a Keplerian fit using the second and the third highest periodogram peaks produced significantly worse folded curves. We have included to perform the fit the RV set computed by López-Santiago (2005). A first fit (see Fig. 13a) derives a close-in massive planet ($a = 0.066$ AU, $M_2 \sin i = 6.54 M_{jup}$) in a circular orbit ($e = 0.05$) with a rotational period of 7.7834 days and a reduced χ^2 of 1.07. Also we present a second fit (see Fig. 13b) with the same period for an eccentric orbit ($a = 0.066$ AU, $M_2 \sin i = 6.15 M_{jup}$, $e = 0.14$, $\chi^2 = 0.997$). Due to the sampling of the data, we cannot discard a possible eccentric orbit.

Orbital elements for both solutions are compiled in Table 4 and discussed in the next section.

As additional test, we computed the orbital solution removing the data affected by flare events. The fit derives a solution ($a = 0.066$ AU, $M_2 \sin i = 6.54 M_{jup}$, $e = 0.01$, $K = 0.91$ km s^{-1}) compatible with the solution when considering all the data. The fit is presented in Fig. 14.

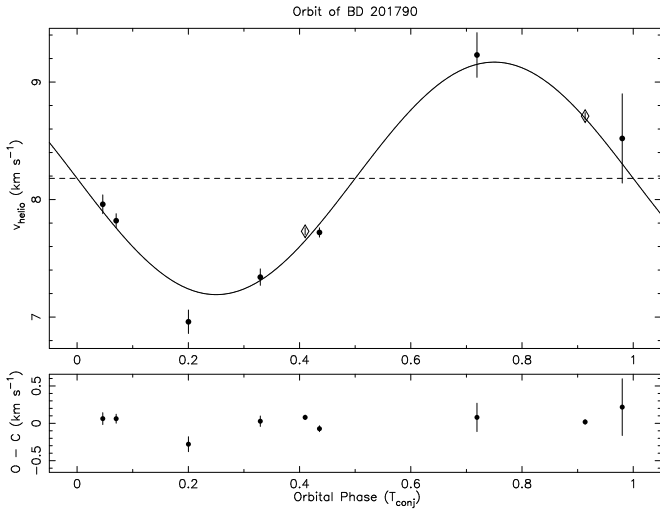


Fig. 14. Radial velocity variation of BD+20 1790 computed considering only the data that are not affected by flares. Circle symbol represent FOCES runs except stars that represent DDT FOCES 08B run. Diamond symbol are for SARG runs.

Table 4. Orbital Parameters of BD+20 1790 b

Parameter	Solution 1	Solution 2	
P_{orb}	7.7834 ± 0.0004	7.7834 ± 0.0004	days
T_{conj}^a	3085.8 ± 0.5	3086.30 ± 0.18	HJD
a	0.066 ± 0.001	0.066 ± 0.002	AU
e	0.05 ± 0.02	0.14 ± 0.04	
K	0.93 ± 0.03	0.84 ± 0.06	km s^{-1}
γ	8.22 ± 0.01	8.12 ± 0.04	km s^{-1}
ω	200.4 ± 21.8	120.7 ± 14.0	degrees
$M_2 \sin i$	6.54 ± 0.57	6.15 ± 0.59	M_{jup}
rms	138.9	132.3	m s^{-1}
χ^2	1.071	0.997	

^a Time of periastron passage

6. Discussion

The lack of a relation between the BIS and spectroscopic indices with the RV period, as well as the different RV and photometrical period strongly suggest that the RV variations are due to a planetary companion. However, it is possible that the RV variations are actually due to a combination of phenomena (activity and planet).

Stellar magnetic activity may be influenced and enhanced by the presence of a close-in giant planet, as proposed by Cuntz et al. (2000), Cuntz & Shkolnik (2002) and Lanza (2008). Thus, the presence of a planetary companion could be an interpretation for the high level of stellar activity detected. In a recent paper, Lanza (2009) proposes a new model that predicts the formation of prominence-like structures in very highly active stars with close-in giant planets. Also, as presented in Sec. 2 and Sec. 4.6, the large flares, with energy releases in the superflare regime, and the high rate of flare occurrence, could find a source in addition to stellar activity in the reconnection of the stellar coronal field as the planet moves inside the Alfvén radius of the star (Ip et al. 2004). In a forthcoming paper we explore in detail these possible star-planet interactions (Hernán-Obispo et al. 2009c, in prep).

In addition, as suggested by the statistical analysis by Kashyap et al. (2008), the X-ray flux from stars with close-in gi-

ant planets is on average 4 times greater than those with more distant planetary companions. For the ‘close-in’ sub-sample, the X-ray luminosity is $L_X = 10^{28.5} \text{ erg s}^{-1}$ on average. The X-ray luminosity of BD+20 1790 is 5 times brighter than this average which is consistent with chromospheric and X-ray emission induced by the presence of a massive close-in companion (Lanza 2009).

Even though the stellar activity could swallow the RV signal of a planetary companion, we can detect it for BD+20 1790 b since it is a massive planet. The RV variation is large enough even though the RV accuracy is typically about 150 m s^{-1} .

Due to the observational strategy (the data are not part of a planet-search program), the eccentricity is poorly constrained. Indeed there is no ‘a priori’ reason to discard an eccentric orbit since the circularization time-scale computed is up to several Gyr, but more data is required to properly characterize the eccentricity. RV optical and infrared follow-up over twice the RV period will enable us to constrain the orbital solution as well as confirm the presence of the planet. More massive exoplanets $M_2 \sin i \sim 5M_{\text{jup}}$ with orbital periods longer than about 6 days have eccentricities significantly larger than lower mass planets (Udry & Santos 2007). Another possibility is that additional undetected longer period planets are maintaining the eccentricity of BD+20 1790 b. Both situations have been discussed in detail by Wu & Murray (2003).

It is worth noting however that the star is metal-rich, as presented in Sec. 2. The existence of a correlation between stellar metallicity and planet mass has been reported by e.g. Santos et al. (2001), Fischer & Valenti (2005), Guillot et al. (2006). Massive planets tend to form around metal-rich stars, i.e., planets that orbit around metal-rich stars also have higher mass cores.

Compared to other planets of similar masses and orbits⁶, and taking into account statistical results described in recent reviews (Udry & Santos 2007), BD+20 1790 b does not exhibit unusual characteristics, except for its young age and its relatively high mass. We used a complimentary method to determine the stellar age from Mamajek & Hillenbrand (2008) (hereafter MH08), that uses the fractional X-ray luminosity, $R_X = L_X/L_{\text{bol}}$. MH08 demonstrate that R_X has the same age-inferring capability as the chromospheric index R'_{HK} . By using their equation [A3] we estimated an age for BD+20 1790 of up to 35 Myr. Considering a value for $\log R'_{\text{HK}} = -4.2$ on average, we can also estimate the age with the new relation proposed by MH08, by equation [3]. We computed an age of up to 58 Myr. These values are in agreement with the range estimated by López-Santiago et al. (2006).

Lowrance et al. (2005) included this star BD+20 1790 in a coronagraphic survey for substellar companions using the coronagraph on NICMOS/HST and the 200 inch Hale Telescope (Palomar Observatory). No companions were found beyond 10 AU. However, the orbital solutions we find suggest a semi-major axis below 0.1 AU, clearly beyond their resolving capabilities.

Great care must therefore be taken when extrapolating properties of early stellar evolution stages from the characteristics of the latter stages, since the current knowledge about planetary system evolution is still somewhat speculative. The exoplanetary zoo is such that new planets with unusual properties require a replanting of planet formation and migration scenarios. Planets discovered around young stars could be the missing link that reconstruct the scenarios between exoplanets and protoplanetary disks. Indeed, further study of BD+20 1790 b has the potential

⁶ Observational data for the more than 370 exoplanets are compiled on the *Extrasolar Planets Encyclopaedia* (<http://exoplanet.eu>), maintained by J. Schneider

to improve our understanding of planetary systems at early evolutionary stages.

7. Conclusions

This paper describes the investigation of RV variations for the young and active K5V star BD+20 1790. Based upon the analysis of the BIS of the CCF, as well as activity indicators and photometry, the presence of a planetary companion is shown to be the best interpretation. The orbital solution results in a companion with a mass in the planetary regime. No photometric period larger than 2.8 days strongly supports the planetary origin of the observed RV variations. Two solutions for the orbit are computed and discussed. The presence of a close-in massive planet could also be an explanation for the high level of stellar activity. Since the RV data are not part of a planet search program, we can consider our results as serendipitous evidence of a planetary companion. Indeed additional RV optical and infrared follow-up will enable us to constrain the orbital solution as well as confirm the presence of the planet. This is thus far the youngest main sequence star for which a planetary candidate has been reported.

Acknowledgements. We thank Calar Alto Observatory for allocation of director's discretionary time to this programme. This work was supported by the Spanish Ministerio de Educación y Ciencia (MEC) under grant AYA2005-02750, Ministerio de Ciencia e Innovación (MICINN) under grant AYA2008-06423-C03-03 and The Comunidad de Madrid under PRICIT project S-0505/ESP-0237 (ASTROCAM). MCGO acknowledges financial support from the European Commission in the form of a Marie Curie Intra European Fellowship (PIEFGA-2008-220679). MHO and GAE thank Dr. Chriss Moss, support astronomer at the LT for his help and patience. Also MHO thanks Dr. Santos Pedraz, support astronomer at the Calar Alto Observatory for his help with DDT run. MHO is grateful to Dr. José Antonio Caballero for valuable discussions, and also Dr. Laurence R. Doyle for his suggestions that was the initial inspiration for this work. This research has made use of the SIMBAD database, operated at CDS, Strasbourg, France. The authors gratefully acknowledge the valuable comments and suggestions of an anonymous referee, that are helped to improve the paper.

References

Barden, S. C., 1985, *ApJ*, 295, 162
 Barnes, J. R., Collier Cameron, A., James, D. J. and Donati, J.-F., 2000, *MNRAS*, 314, 162
 Barnes, J. R., Cameron, A. C., et al., 2005, *MNRAS*, 356, 1501
 Biazzo, K., Frasca, A., Henry, G. W. et al., 2007, *ApJ*, 656, 474
 Bonfils, X., Mayor, M., Delfosse, X. et al., 2007, *A&A*, 474, 293
 Bouvier, J., Alencar, S. H. P., Bouletier, T., et al., 2007, *A&A*, 463, 1017
 Byrne, P. B., Eibe, M. T. and Rolleston, W. R. J., 1996, *A&A*, 311, 651
 Cardiel, N., 1999, PhD Thesis, Universidad Complutense de Madrid
 Carpenter, J. M., Bouwman, J., Silverstone, M. D. et al., 2008, *ApJS*, 179, 423
 Carroll, B. W. and Ostlie, D. A., 2007, *An Introduction to Modern Astrophysics*, 2nd edition, Pearson International Edition, Addison Wesley
 Catalano, S., Biazzo, K., Frasca, A. et al., 2002, *A&A*, 394, 1009
 Collier Cameron, A. and Robinson, R. D., 1989a, *MNRAS*, 236, 57
 Collier Cameron, A. and Robinson, R. D., 1989b, *MNRAS*, 238, 657
 Collier Cameron, A. and Woods, J. A., 1992, *MNRAS*, 258, 360
 Collier Cameron, A., 1997, *MNRAS*, 287, 556
 Collier Cameron, A., 2001, in *IAU Symposium*, "Recent Insights into the Physics of the Sun and Heliosphere: Highlights from SOHO and Other Space Missions", 203, p229
 Collier Cameron, A., Jardine, M. M. and Donati, J.-F., 2002, in *ASP Conf. Ser.*, "Stellar Coronae in the Chandra and XMM-NEWTON Era", 277, p397
 Cumming, A., 2004, *MNRAS*, 354, 1165
 Cuntz, M. and Saar, S. H. and Musielak, Z. E., 2000, *ApJ*, 533, L151
 Cuntz, M. and Shkolnik, E., 2002, 323, 387
 Desort, M., Lagrange, A.-M. et al., 2007, *A&A*, 473, 983
 Donati, J.-F., Mengel, M., Carter, B. D. et al., 2000, *MNRAS*, 316, 699
 Eibe, M. T., 1998, *A&A*, 337, 757
 Eibe, M. T., Byrne, P. B., Jeffries, R. D. et al., 1999, *A&A*, 341, 527
 Esposito, M., Guenther, E., Hatzes, A. P. et al., 2006, "Tenth Anniversary of 51 Peg-b: Status of and prospects for hot Jupiter studies", p127
 Ferreira, J. M., 2000, *MNRAS*, 316, 647

Fischer, D. A. and Valenti, J., 2005, *ApJ*, 622, 1102
 Fleming, T. A., Schmitt, J. H. M. M. and Giampapa, M. S., 1995, *ApJ*, 450, 401
 Frasca, A., Biazzo, K., Catalano, S. et al., 2005, *A&A*, 432, 647
 Gratton, R. G., Bonanno, G., Bruno, P. et al., 2001, *Exp. Ast.*, 12, 107
 Gonzalez, G., Laws, C., Tyagi, S. et al., 2001, *AJ*, 121, 432
 Guillot, T., Santos, N. C., Pont, F. et al., 2006, *A&A*, 453, L21
 Hernán-Obispo, M., de Castro, E., Cornide, M., 2005, *ESA Special Publication*, 560, 647
 Hernán-Obispo, M., de Castro, E., Gálvez, M.C., "Highlights of Spanish Astrophysics IV", 2007, Kluwer Academic Publishers
 Houdebine, E. R., 1992, *Irish Astronomical Journal*, 20, 213
 Huelamo, N., Figueira, P. et al., 2008, *ArXiv e-prints*, 0808.2386
 Huerta, M., Johns-Krull, C. M. et al., 2008, *ApJ*, 678, 472
 Ip, W.-H., Kopp, A. and Hu, J.-H., 2004, *ApJ*, 602, L53
 Jardine, M., Collier Cameron, A., Donati, J.-F. et al., 2001, *MNRAS*, 324, 201
 Jardine, M. and van Ballegooijen, A. A., 2005, *MNRAS*, 361, 1153
 Jeffries, R. D. and Jewell, S. J., 1993, *MNRAS*, 264, 106
 Jeffries, R. D., Byrne, P. B., Doyle, J. G. et al., 1994, *MNRAS*, 270, 153
 Jeffries, R. D. 1995, *MNRAS*, 273, 559
 Kashyap, V. L., Drake, J. J. and Saar, S. H., 2008, *ApJ*, 687, 1339
 Kurucz, R. L., 1993, *IAU Colloq. 138: Peculiar versus Normal Phenomena in A-type and Related Stars*, APCS, 44, 87
 Kürster, M., Endl, M., Rouesnel, F. et al., 2003, *A&A*, 403, 1077
 Lanza, A. F., 2008, *A&A*, 487, 1163
 Lanza, A. F., 2009, *A&A*, 505, 339
 López-Santiago, J., 2005, PhD Thesis, Universidad Complutense de Madrid
 López-Santiago, J., Montes, D., Crespo-Chacón, I., et al., 2006, *ApJ*, 643, 1160
 Lowrance, P. J., Becklin, E. E., Schneider, G., Kirkpatrick, et al., 2005, *AJ*, 130, 1845
 Mamajek, E. E. and Hillenbrand, L. A., 2008, *ApJ*, 687, 1264
 Mason, K. O., Hassall, B. J. M., Bromage, G. E. et al., 1995, *MNRAS*, 274, 1194
 Martín, E. L., Guenther, E., Zapatero Osorio, M. et al., 2006, *ApJ*, 644, L75
 Martínez Fiorenzano, A. F., Gratton, R. G., Desidera, S. et al., 2005, *A&A*, 442, 775
 Mayor, M. and Queloz, D., 1995, *Nature*, 378, 355
 Montes, D., de Castro, E., Fernandez-Figueroa, M. J. et al., 1995, *A&AS*, 114, 287
 Norton, A. J., Wheatley, P. J., West, R. G., et al., 2007, *A&A*, 467, 785
 Paulson, D. B., Cochran, W. D. and Hatzes, A. P., 2004, *AJ*, 124, 3579
 Paulson, D. B. and Yelda, S., 2007, *PASP*, 118, 706
 Pfeiffer, M. J., Frank, C., Baumüller, D. et al., 1998, *A&AS*, 130, 381
 Prato, L., Huerta, M., Johns-Krull, C. M. et al., 2008, *ApJ*, 687, L103
 Queloz, D., Henry, G. W., Sivan, J.P., et al., 2001, *A&A*, 379, 279
 Reid, I. N., Cruz, K. L., Allen, P. et al., 2004, *AJ*, 128, 463
 Rubenstein, E. P. and Schaefer, B. E., 2000, *ApJ*, 529, 1031
 Santos, N. C., Mayor, M., Naef, D. et al., 2000, *A&A*, 361, 265
 Santos, N. C., Israelian, G. and Mayor, M., 2001, 373, 1019
 Saar, S. H. and Donahue, R. A., 1997, *ApJ*, 485, 319
 Saar, S. H. and Fischer, D., 2000, *ApJ*, 534, L105
 Saar, S. H., 2003, in *Astronomical Society of the Pacific Conference Series* "Scientific Frontiers in Research on Extrasolar Planets", 294, p65
 Saar, S. H., 2009, *American Institute of Physics Conference Series*, 1094, 152
 Scargle, J. D., 1982, *ApJ*, 263, 835
 Setiawan, J., Weise, P., Henning, T., et al., 2007, *ApJ*, 660, L145
 Setiawan, J., Henning, T. and Launhardt, R. et al., 2008, *Nature*, 451, 38
 Sneden, C., 1973, *ApJ*, 184, 839
 Steele, I. A., Smith, R. J., Rees, P. C. et al., 2005, "Society of Photo-Optical Instrumentation Engineers (SPIE) Conference Series", 5489, 679
 Tonry, J. and Davis, M., 1979, *AJ*, 84, 1511
 Udry, S., Santos, N. C., 2007, *ARA&A*, 45, 397
 Walter, F. M., 1994, in *IAU Symposium* "Stellar Surface Structure", 176, p355
 Wu, Y., Murray, N., 2003, *ApJ*, 589, 605

Appendix A: Periodogram

We use a Least squares periodogram approach to identify and visually illustrate the relevant periods in the data. It differs from the more classic Lomb-Scargle periodogram (Scargle 1982) in a few key aspects. For a given period P , a linear model of the form $v_r = \gamma + A \cos 2\pi/Pt + B \sin 2\pi/Pt$ is fitted using a weighted least squares to the data and the χ^2 of the residuals is obtained. The χ^2 minima reveal the candidate signals of interest. One can represent the root mean square of the residuals (RMS) with respect to the period to show the relevant periods as minima (This approach is used to illustrate the photometric periods in Fig. 3). To

recover a more familiar view of a periodogram, one can compute the *Power* of each period P as

$$\text{Power}(P) = \frac{(\chi_{\text{none}}^2 - \chi_P^2)/2}{\chi_P^2/(n_{\text{obs}} - 3)} \quad (\text{A.1})$$

$$\chi_{\text{none}}^2 = \sum_i^{\text{obs}} \left(\frac{v_i - \langle v \rangle}{\sigma} \right)^2 \quad (\text{A.2})$$

that follows a Fisher-F Distribution with 2 and $n_{\text{obs}} - 3$ degrees of freedom and can be used to obtain a first hint of the False Alarm probability of a given solution. This definition of the power measures how much the χ^2 of the fit improves when a sinusoid of period P is included (see Cumming 2004 for a more detailed description).

Since analytical approaches tend to give optimistic confidence levels, it is desirable to obtain the False Alarm Probability of a solution empirically. To make this, we generate a large number of synthetic datasets (10^5) with the same sampling cadence (same dates) but only containing random noise. Then, for each realization, we compute the Least Squares periodogram and find the period with higher power, which will be a false alarm. A histogram of False Alarms as a function of the Power is obtained and its complementary cumulative distribution gives the False Alarm Probability of a given peak in our signal. The Least Squares periodogram of the RVS data and its associated empirical FAP probability distribution are shown in Fig. 4. Compared to the Lomb-Scargle periodogram, this approach allows a proper weighting of each observation and can be easily generalized to include other time-dependent effects in the signal at the period search level.